Published in final edited form as:
Nat Immunol. 2014 January ; 15(1): 88–97. doi:10.1038/ni.2771.

Dominant-Activating, Germline Mutations in Phosphoinositide 3-Kinase p110δ Cause T Cell Senescence and Human Immunodeficiency

Carrie L. Lucas[1,15], **Hye Sun Kuehn**[2,15], **Fang Zhao**[3,14,15], **Julie E. Niemela**[2], **Elissa K. Deenick**[4,5], **Umaimainthan Palendira**[4,5], **Danielle T. Avery**[4], **Leen Moens**[4], **Jennifer L. Cannons**[3], **Matthew Biancalana**[1], **Jennifer Stoddard**[2], **Weiming Ouyang**[6], **David L. Frucht**[6], **V. Koneti Rao**[1], **T. Prescott Atkinson**[7], **Anahita Agharahimi**[8,9], **Ashleigh A. Hussey**[8], **Les R. Folio**[10], **Kenneth N. Olivier**[8], **Thomas A. Fleisher**[2], **Stefania Pittaluga**[11], **Steven M. Holland**[8], **Jeffrey I. Cohen**[12], **Joao B. Oliviera**[13], **Stuart G. Tangye**[4,5], **Pamela L. Schwartzberg**[3], **Michael J. Lenardo**[1], and **Gulbu Uzel**[8]

[1]Molecular Development of the Immune System Section, Laboratory of Immunology, National Institute of Allergy and Infectious Diseases, National Institutes of Health, Bethesda, MD, USA

Correspondence should be addressed to G.U. (guzel@niaid.nih.gov).
[15]These authors contributed equally.

ACCESSION CODE
OMIM: 602839

AUTHOR CONTRIBUTIONS
C.L.L performed experiments, analyzed data, and developed and wrote the manuscript.
H.S.K. performed experiments and analyzed data.
F.Z performed experiments and analyzed data.
J.E.N. performed genomic DNA sequencing analysis, bioinformatics analysis, candidate gene discovery, and protein structure analysis.
E.K.D. performed experiments and analyzed data.
U.P. performed experiments and analyzed data.
D.T.A. performed experiments and analyzed data.
L.M. performed experiments and analyzed data.
J.L.C. performed experiments and analyzed data.
M.B. performed p110 structural analysis.
J.S. performed experiments, genomic DNA sequencing analysis, and data analysis.
W.O. performed experiments.
D.L.F. supervised research and data analysis.
V.K.R. evaluated patients and collected data.
T.P.A. provided patient access, clinical data, samples, and advice.
A.A. evaluated patients and collected and analyzed data.
A.A.H. coordinated patient access, data collection and analysis.
L.R.F. evaluated and prepared data from clinical imaging studies.
K.N.O. evaluated patients and collected and analyzed data.
T.A.F. supervised research and data analysis and provided advice.
S.P. performed histological and immunohistochemical analyses of patient samples.
S.M.H. supervised research and data analysis and provided advice.
J.I.C. provided patient access, clinical data, samples, and advice.
J.B.O planned and supervised whole exome sequencing experiments.
S.G.T. planned and supervised experiments, analyzed data, provided advice, and prepared the manuscript.
P.L.S. planned and supervised experiments, analyzed data, and provided advice.
M.J.L. supervised research and data analysis, provided advice, and prepared the manuscript.
G.U. coordinated research efforts, supervised research work and data analysis, and prepared the manuscript.
All authors discussed and revised the manuscript.

[2]Department of Laboratory Medicine, Clinical Center, National Institutes of Health, Bethesda, MD, USA

[3]Cell Signaling Section, Genetic Disease Research Branch, National Human Genome Research Institute, National Institutes of Health, Bethesda, MD, USA

[4]Immunology and Immunodeficiency Group, Immunology Program, Garvan Institute of Medical Research, Sydney, Australia

[5]St. Vincent's Clinical School Faculty of Medicine, University of New South Wales, Sydney, Australia

[6]Laboratory of Cell Biology, Division of Monoclonal Antibodies, Office of Biotechnology Products, Center for Drug Evaluation and Research, United States Food and Drug Administration, Bethesda, Maryland, USA

[7]Division of Allergy and Immunology, Department of Pediatrics, University of Alabama at Birmingham, Birmingham, AL, USA

[8]Laboratory of Clinical Infectious Diseases, National Institute of Allergy and Infectious Diseases, National Institutes of Health, Bethesda, MD, USA

[9]Support to Laboratory of Clinical Infectious Diseases, Clinical Research Directorate/CMRP, SAIC-Frederick, Frederick National Laboratory for Clinical Research, Frederick, MD, USA

[10]Radiology and Imaging and Sciences Clinical Center, National Institutes of Health, Bethesda, MD, USA

[11]Laboratory of Pathology, National Cancer Institute, National Institutes of Health, Bethesda, MD, USA

[12]Laboratory of Infectious Diseases, National Institute of Allergy and Infectious Diseases, National Institutes of Health, Bethesda, MD, USA

[13]Instituto de Medicina Integral Prof. Fernando Figueira-IMIP, Recife-PE, Brazil

[14]Pritzker School of Medicine, The University of Chicago, Chicago, IL, USA

Abstract

The p110δ subunit of phosphoinositide 3-kinase (PI(3)K) is selectively expressed in leukocytes and is critical for lymphocyte biology. Here we report three different germline, heterozygous, gain-of-function mutations in the *PIK3CD* gene encoding p110δ in fourteen patients from seven families. These patients presented with sinopulmonary infections, lymphadenopathy, nodular lymphoid hyperplasia and CMV and/or EBV viremia. Strikingly, naïve and central memory T cells were severely deficient, while senescent effector T cells were over-represented. *In vitro*, patient T cells exhibited increased phosphorylation of Akt and hyperactivation of mTOR, enhanced glucose uptake and terminal effector differentiation. Importantly, treatment with rapamycin to inhibit mTOR activity *in vivo* partially restored naïve T cells, largely rescued the *in vitro* T cell defects, and improved clinical course.

The phosphoinositide 3-kinase (PI(3)K) pathway plays crucial roles throughout eukaryotic biology. In mammals, there are three classes of PI(3)K that are distinct in their mechanisms of regulation, substrate specificity and structure[1]. All classes of PI(3)K phosphorylate the inositol ring of phosphatidylinositol lipids in membranes, and several of these enzymes can also phosphorylate protein substrates at serine/threonine residues[2]. Class I PI(3)Ks play the largest role in immune cells and are composed of a catalytic p110 subunit and a regulatory p85 subunit that governs the stability, membrane localization and activity of p110. Among the class I PI(3)K molecules, only p110δ (OMIM: 602839) is restricted to leukocytes[3,4] and has specialized functions in adaptive immunity. Activation of p110δ requires ligation of cell surface receptors linked to tyrosine kinase activity, leading to recruitment of the PI(3)K complex to pYxxM motifs via two Src-homology 2 (SH2) domains in the regulatory p85 subunit[5]. Binding of p85 to phosphorylated tyrosine relieves its inhibition of p110, resulting in p110-mediated phosphorylation of phosphatidylinositol (4,5) bis-phosphate (PtdIns(4,5)P_2) to generate phosphatidylinositol (3,4,5) triphosphate (PtdIns(3,4,5)P_3), which initiates plasma membrane recruitment of Pleckstrin Homology (PH) domain-containing signaling proteins. Negative regulators of PI(3)K include phosphatase and tensin homolog (PTEN) and SH2 domain-containing inositol 5′-phosphatase (SHIP), which convert PtdIns(3,4,5)P_3 to PtdIns(4,5)P_2 and PtdIns(3,4)P_2, respectively. Despite a vast literature on PI(3)K, the basic question of how p110δ activity modulates human immunity remains unanswered.

T cell function is heavily dependent on regulation of cellular metabolism to control proliferative capacity, effector function and generation of memory[6]. The mechanistic target of rapamycin (mTOR) kinase, which is activated by PI(3)K, plays a prominent role in promoting dynamic changes in T cell metabolism[7,8]. PI(3)K has been described to activate the mTOR complex 2 (mTOR, Rictor and GβL) by promoting its association with ribosomes[9]. Moreover, PtdIns(3,4,5)P_3 generated by PI(3)K recruits both phosphoinositide-dependent kinase 1 (PDK1) and protein kinase B (PKB, also known as Akt), thereby enabling full activation of Akt through phosphorylation at T308 (by PDK1) and S473 (by mTORC2)[10,11]. In its active form, Akt activates mTOR complex 1 (mTOR, Raptor and GβL), leading to phosphorylation of 4EBP1 and p70S6K to promote protein translation[12]. Phosphorylation of 4EBP1 results in its release from eIF4E and promotes cap-dependent translation, whereas phosphorylation of p70S6K activates the ribosomal S6 protein to enhance translation of ribosomal proteins and elongation factors. One of the proteins whose expression is increased by mTORC1 activity is HIF-1α, a key regulator of glycolysis[13]. As such, in cells with high PI(3)K-Akt-mTOR activity, a metabolic shift toward glycolysis would be expected and, indeed, this occurs upon differentiation of naïve T cells into effector T cells[14]. In addition to HIF-1α, mTORC1 activity promotes p53 translation and protein stability and has been linked to the role of p53 in inducing cellular senescence[15]. However, it is unknown how constitutive activation of the Akt-mTOR pathway affects T cell function and immunity in humans.

Upon encounter of a naïve T cell with antigen, a differentiation process ensues to generate both short-lived effector cells to respond to the acute phase of infection as well as long-lived memory cells to ensure a rapid and vigorous immune response if the same antigen is re-encountered. For $CD8^+$ T cells, the Akt-mTOR pathway has been highlighted as a critical

mediator of short-lived effector cell (SLEC) versus memory precursor effector cell (MPEC) differentiation[16]. When Akt-mTOR signaling is sustained, a transcriptional program promoting effector function drives cells toward differentiation into terminal effectors at the expense of memory formation[17,18]. Evidence has mounted to suggest that effector cells must "reset" their metabolic activity to become memory cells. Naïve $CD8^+$ T cells use fatty acid oxidation and mitochondrial respiration to meet their relatively low energy demands; however, following activation of naïve cells, a switch to lipid synthesis and glycolysis is necessary to rapidly provide the cell with sufficient energy to carry out effector functions. To survive and contribute to the memory pool, effector $CD8^+$ T cells must revert back to the catabolic processes of fatty acid oxidation and mitochondrial respiration[12]. The Akt-mTOR pathway is a central mediator of this switch since it promotes glucose uptake, glycolysis and lipid synthesis, all processes crucial for the differentiation of $CD8^+$ T cells[19]. Therefore, it is of great interest to determine how alterations in these metabolic pathways in immune cells can affect T cell differentiation and human health.

Here we describe a group of patients with combined immunodeficiency and lymphoproliferative disease who share gain-of-function mutations in the *PIK3CD* gene encoding PI(3)K p110δ. These mutations result in hyperactivation of mTOR signaling and skewed differentiation of $CD8^+$ T cells to short-lived effector cells with severely impaired memory T and B cell development.

RESULTS

Immunodeficiency, proliferation and memory abnormalities

We evaluated nine patients from seven unrelated families of different ethnic and racial backgrounds who presented with childhood onset sinopulmonary infections, lymphoproliferation (Supplementary Fig. 1a,b), chronic Epstein-Barr Virus (EBV) and/or Cytomegalovirus (CMV) viremia, and distinctive nodular lymphoid ($CD3^+$ and $CD20^+$) hyperplasia of mucosal surfaces (Table 1 and Supplementary Table 1, Fig. 1a and Supplementary Fig. 1). Autoimmune cytopenias were also observed in several patients (Supplementary Table 1). Of relevance, EBV-driven B cell lymphoma occurred in two index patients (C.1 and F.II.1), one of whom (F.II.1) was diagnosed with EBV^+ nodular sclerosis form of classical Hodgkin lymphoma (Fig. 1b), which is characteristically observed in immunodeficient patients[20]. Additionally, a 12-year-old patient (B.III.1) with extensive non-malignant lymphoproliferation represents the third generation of a family in which two other members had EBV-associated lymphomas (supporting an autosomal-dominant inheritance pattern). Although lymph node architecture was preserved, B cell follicles showed prominent germinal centers with absent mantle zones and no detectable IgG staining (Fig. 1c). Notably, the peripheral blood B cell compartment lacked memory $CD27^+$ B cells and was enriched in immature transitional $CD10^+$ B cells (Fig. 1d). We observed progressive $CD4^+$ T cell lymphopenia (Fig. 1e) with normal to high $CD8^+$ T cell counts (Fig. 1f and Table 1). Patient T cell responses were poor to *in vitro* mitogen stimulation (Supplementary Fig. 1c) and recall challenge to tetanus (Fig. 1g). Intriguingly, we found a reversed CD4/CD8 ratio and severely reduced $CD45RA^+CCR7^+$ naïve and $CD45RA^-CCR7^+$ central memory T cells (T_{CM}) with a corresponding increase in $CD45RA^-CCR7^-$ effector memory

T cells (T_{EM}) and CD45RA$^+$ effector memory (T_{EMRA}) T cells (Fig. 1h,i and Supplementary Fig. 1d).

Since patients present with sinopulmonary infections and show a deficiency in memory and overrepresentation of transitional B cells (Fig. 1d), we further investigated these lymphocytes. Alterations in serum immunoglobulin concentrations were observed in patients, most with normal to elevated IgM and reduced IgA concentrations (Supplementary Fig. 1e). Serum IgG concentrations were variable, but specific antibody titers were consistently low in patients (data not shown). We observed a normal frequency of total B cells in the blood (Supplementary Fig. 2a) but increased expression of IgM (not shown) and CD5 (Supplementary Fig. 2b), a marker downregulated as B cells mature, on both transitional and naïve B cells from patients. Consistent with the histology data (Fig. 1c), the contracted population of memory B cells in patient peripheral blood had severely reduced frequencies of class-switched IgG$^+$ and IgA$^+$ cells (Supplementary Fig. 2c). *In vitro* analysis of naïve B cell function revealed that they could undergo near-normal proliferation in response to a variety of stimuli (Supplementary Fig. 2d), acquire expression of *AICDA* (the gene encoding activation-induced cytidine deaminase, AID) (Supplementary Fig. 2e), and secrete IgM (Supplementary Fig. 2f, left). However they were impaired in secreting class switched immunoglobulin isotypes (Supplementary Fig. 2f, middle and right). Memory B cells behaved similarly, with normal secretion of IgM, but impaired IgG and IgA production (Supplementary Fig. 2g). These latter findings are consistent with the *in vivo* data demonstrating reduced serum immunoglobulin and impaired humoral immune responses, leading to susceptibility to sinopulmonary infections. Thus, this cohort of patients has combined T and B cell immunodeficiency, impaired memory T cell responses with lymphoproliferation, and a striking inability to control EBV and CMV infections.

Heterozygous, gain-of-function mutations in PIK3CD

PIK3CD encodes PI(3)K p110δ, a protein of 1,044 amino acids with at least five domains identified by structure and function: adapter binding domain (ABD), Ras binding domain (RBD), the PI(3)K-type C2 domain, helical domain, and a kinase domain with amino (N) and carboxy (C) side lobes (Fig. 2a). Using whole exome[21] and targeted Sanger sequencing, we detected in fourteen of our patients and family members the following three heterozygous *PIK3CD* mutations, each located in a different domain (notation based on NM_005026). One index patient possessed a mutation at cDNA position 1002 (C>A) resulting in a N334K amino acid substitution in the C2 domain. Seven patients (three index patients plus four affected relatives, 2 of whom have not been fully evaluated) had a mutation at nucleotide 1573 (G>A), resulting in a E525K substitution in the helical domain. Six patients (three index patients plus three deceased, affected relatives) possessed a mutation at 3061 (G>A), causing a E1021K substitution in the C-lobe of the kinase domain (Fig. 2a,b). All individuals carrying a mutation were found to have characteristics of the disease upon evaluation. The three mutations were predicted to be damaging by functional prediction algorithms including SIFT, PP2, LRT, MutationTaster, and MutationAssessor. The mutations were suspected to be gain-of-function (GOF) mutations based on protein structure analysis and comparison to homologous GOF mutations in p110α described in human cancer cells (Supplementary Fig. 3 and Supplementary Table 3)[22]. Since p110δ and

p110α share substantial amino acid homology, as noted above, we could confidently map the patient N334K and E525K p110δ mutation to the same amino acid substitutions at the homologous residues 345 and 545, respectively, of mutant p110α previously described as GOF mutations in cancer[22–25]. The E1021K (kinase domain) mutation was previously reported in a boy with primary B cell immunodeficiency[26]. Amino acid E1021 of p110δ corresponds with D1045 of p110α, which is two residues upstream of a known GOF mutation (p110α H1047R) that reportedly increases interaction of p110α with the cell membrane, thereby increasing its activity by enhancing accessibility of the binding site to PtdIns(4,5)P_2 (ref. 23). The change from E to K at residue 1021 of p110δ results in a similar pKa change (+6.28) as that for the H to R change at residue 1047 of p110α (+6.48), predicting the same increased propensity for interaction with the negatively charged phospholipid head groups of the interior cell membrane. Moreover, two additional reports demonstrate that the p110α H1047R mutation mimics binding to Ras-GTP to augment PI(3)K catalytic activity[25] and affects the conformation of the activation loop to promote kinase activity[22], suggesting that the E1021K p110δ mutation in our patients may have multiple GOF effects.

Only two of the seven families were confirmed to have a *de novo* mutation in the index patient, and another three had confirmed affected individuals in multiple generations (Fig. 2c). For the remaining two families, specimens from one or both parents were not accessible. The appearance of *PIK3CD* mutations in three different sites among seven unrelated families from different ethnic and racial backgrounds (Supplementary Table 1) eliminates the possibility of a founder effect, while the presence of the same mutation in multiple families suggests the occurrence of mutational hot spots, as seen previously in genetic diseases of the immune system[27,28].

Next, we sought to evaluate expression of p110δ and test the hypothesis that PI(3)K is hyperactive in our patients. We examined p110δ protein abundance and S473 phosphorylation of Akt in patient T cell blasts and peripheral blood mononuclear cells (PBMCs) (Fig. 2d and Supplementary Fig. 4a–c). Expression of the mutant p110δ protein was normal; however, phosphorylation of Akt was increased before and after anti-CD3 stimulation (Supplementary Fig. 4a). We also found that phosphorylation of residue T308 of Akt was increased in patient T cell blasts (Supplementary Fig. 4d,e). Moreover, Foxo1, a substrate of Akt that is degraded upon its phosphorylation, was lower in patient T cell blasts compared to healthy controls by immunoblot analysis (data not shown). To confirm that p110δ mutations are responsible for this cellular phenotype, we overexpressed the N334K, E525K, and E1021K patient p110δ proteins in normal human PBMCs and found that the mutant p110δ proteins induced hyper-phosphorylation of Akt (Fig. 2e and Supplementary Fig. 4f). This result was also confirmed by overexpression of mutant p110δ in the H9 T cell line (Supplementary Fig. 4g). Moreover, we found that mutant p110δ could interact with p85α as well as wild-type p110δ, as assessed by overexpression and co-immunoprecipitation (Supplementary Fig. 4h). Thus, each individual in our patient cohort carries an inherited or *de novo* heterozygous, GOF mutation in the gene encoding p110δ, leading to expression of a hyperactive kinase that augments Akt phosphorylation.

Expanded CD8 T cells with senescent terminal differentiation

We next examined EBV-specific $CD8^+$ T cell frequencies by staining *ex vivo* PBMCs with HLA tetramers loaded with lytic or latent EBV peptide antigens. Despite uncontrolled EBV, these patients generated normal to high frequencies of EBV-specific $CD8^+$ T cells (Fig. 3a and Supplementary Fig. 5a). Tetramer-positive $CD8^+$ T cells had a memory phenotype ($CD45RA^-$) and were more activated, as shown by CD38 upregulation, compared to controls (Supplementary Fig. 5b,c). These data suggest that the *PIK3CD* mutations are unlikely to be globally impairing *in vivo* antigen recognition by T cells.

Phenotypically, patient $CD8^+$ T cells appeared to be predominantly CCR7-negative cells, suggesting a terminally differentiated state (Fig. 1h and Supplementary Fig. 1d). Correspondingly, *in vitro* activation of whole PBMCs (but not isolated naïve $CD4^+$ T cells) with various stimuli revealed a reduced proliferative capacity and diminished interleukin 2 (IL-2) secretion (Fig. 3b,c), though the proliferation defect could be overcome by stimulation with anti-CD2/3/28 beads or allogeneic PBMC plus PHA (data not shown). Since the composition of cells in the peripheral blood of patients is biased toward effector T cells, this finding is consistent with the well-described ability of naïve T cells to proliferate better than differentiated effectors. Also consistent with a T_{EM}/T_{EMRA} phenotype, activated patient $CD8^+$ T cells exhibited enhanced markers of effector functions. We found that expression of interferon-γ IFN-γ), T-bet and granzyme B, as well as degranulation, as reflected by LAMP1 (also called CD107a) cycling after stimulation, were all increased in cytotoxic T lymphocytes (CTLs) cultured from patients compared to those from normal controls (Fig. 3d–f and Supplementary Fig. 5d–f). We also assessed granzyme B expression after activation of purified naïve $CD8^+$ T cells and, again, observed higher expression in patient compared to healthy control cells (data not shown). When cytotoxic function of patient CTLs was examined using anti-CD3-mediated redirected lysis of P815 targets, patient cells exhibited a normal capacity to kill (Supplementary Fig. 5g). Intriguingly, we found that expression of the senescence-associated marker CD57 was significantly higher on patient $CD8^+$ but not $CD4^+$ T cells (Fig. 3g, Supplementary Fig. 5h and Table 1)[29]. Of note, we observed normal to high expression of NKG2D (not shown) and variable PD-1 expression on patient $CD8^+$ T cells (Supplementary Fig. 6). Hence, phenotypically and functionally, patient $CD8^+$ T cells were mostly T_{EM}/T_{EMRA} with a low proliferative capacity but possessing certain aspects of high effector function characteristic of senescent effector cells.

Augmented mTOR signaling and glycolysis

To gain insight into how p110δ GOF mutations cause terminal differentiation and senescence, we examined signaling pathways downstream of PI(3)K. TCR-induced calcium flux and NF-κB p65 nuclear translocation in patient T cell blasts were normal, demonstrating that multiple aspects of TCR signaling were intact (Fig. 4a,b). Moreover, the expression of PTEN, p27kip1, and other signaling molecules was normal in patient T cells (Supplementary Fig. 7). An important molecule activated downstream of PI(3)K and Akt in many cell types is mTOR, a serine/threonine kinase that modulates T cell metabolism and $CD8^+$ T cell effector differentiation through induction of glycolysis. We therefore hypothesized that hyperactive PI(3)K-Akt signaling was affecting T cell metabolism by

stimulating the mTOR pathway. Consistent with this hypothesis, we observed increased S235/S236 phosphorylation of the ribosomal S6 protein downstream of mTOR in activated patient cells compared to controls (Fig. 4c,d and Supplementary Fig. 8a), and this was true even when naïve $CD8^+$ T cells were purified and activated (data not shown). To confirm that the increased S6 phosphorylation in patient cells is through mTORC1, we also examined extent of phosphorylation at the mTORC1-specific[30] sites S240/S244 of S6 (Fig. 4e). Similar to the S235/S236 sites, the S240/244 sites on S6 were hyperphosphorylated in cultured patient T cell blasts. Moreover, this phosphorylation was greatly reduced by inhibition of either p110δ or mTORC1 using IC87114 or rapamycin, strongly supporting the conclusion that hyperactive PI(3)K is driving hyperactivation of mTOR in patient cells. As further support, we measured S235/S236 phosphorylation of S6 but pre-incubated cells in phosphate-buffered saline (PBS) to remove the glucose and amino acids required to maintain mTOR activity. Indeed, we found that the hyperphosphorylation of S6 observed was lost under these conditions (Supplementary Fig. 8b), consistent with a requisite role for mTOR in S6 hyperphosphorylation. As hypothesized from mTORC1 hyperactivation, glucose uptake was augmented in T cell blasts from p110δ mutant patients compared to normal controls (Fig. 4f and Supplementary Fig. 8c). Increased glucose uptake was also evident in lymph nodes of patient G.1 as evaluated by positron emission tomography (PET) scan (Fig. 4g), suggesting mutant p110δ is driving T cells into glycolytic metabolism. Interestingly, the most clinically affected patients (A.1 and G.1) also had the most hyperphosphorylation of S6 and greatest glucose uptake. Thus, activating p110δ mutations are associated with hyperactivity of the PI(3)K-Akt-mTOR signaling pathway in T cells, which leads to enhanced glycolysis, providing a mechanism for the predisposition to senescence.

Treatment of disease with rapamycin

Since aerobic glycolysis is induced after T cell activation[6] and is incompatible with maintenance of resting naïve and memory T cells[12], we hypothesized that *in vivo* treatment of p110δ mutant patients with rapamycin to inhibit mTOR (and therefore glycolysis) would enable persistence of naïve and memory T cells. Upon treatment of patient A.1, the most severely affected patient with extreme lymphoproliferation, with rapamycin (trough drug concentrations equaling 15 ng/ml), we observed a reduction in $CD8^+$ T cell counts to normal numbers within approximately four months and noted an increase in percentage of naïve T cells in PBMC samples (Fig. 5a,b). This effect was specific since $CD4^+$ T cells, which were not expanded in the patients, showed no decrease in number after rapamycin therapy (Fig. 5a). Consistent with rescue of naïve T cells in the peripheral blood, we found a near complete restoration of IL-2 secretion and proliferative response after *in vitro* TCR ligation (Fig. 5c,d). Clinically, we observed a reduction in hepatospenomegaly and lymphadenopathy (Supplementary Fig. 9). Thus, *in vivo* administration of an mTOR inhibitor improves immune derangements induced by GOF mutation in p110δ, most likely by modulating the cell populations in patient blood to restore a more normal balance of naïve, effector and memory $CD8^+$ T cell populations. Taken together, these data support the hypothesis that enhanced activity of p110δ due to a genetic alteration elicits a lymphoproliferative immunodeficiency caused by mTOR-dependent skewing of T cells to a

senescent effector phenotype (Fig. 6), which can be reversed pharmacologically by rapamycin.

DISCUSSION

Studies in animal models have suggested that impaired PI(3)K signaling leads to immunodeficiency and inflammation, whereas unrestrained PI(3)K signaling contributes to autoimmunity and hematological malignancy[1]. However this simplistic dichotomy does not fully explain the effects of PI(3)K. Mice expressing a catalytically inactive form of p110δ exhibited impaired antigen receptor signaling in B and T cells and attenuated immune responses but also developed inflammatory bowel disease[31]. Moreover, mice lacking p85α showed impaired B cell development and activation but normal T cell activation under the conditions tested[32,33]. Similarly, patients deficient in the p85α subunit of PI(3)K also lacked B cells and serum immunoglobulins[34]. T cell–specific deletion of PTEN in mice resulted in hyperactivation of the PI(3)K pathway and caused a lethal lymphoproliferative disease[35]. In human cancers, activating mutations in PI(3)K proteins (most frequently p110α) are common, consistent with their role in proliferation and survival[36,37]. Enhanced PI(3)K activity has also been observed in hematopoietic cancers due to oncogenic activation of upstream regulators[38], prompting investigation of p110δ-specific inhibitors for therapeutic use[39]. However, the full phenotypic effect of inherited genetic lesions in p110δ in humans has not been described. We now report identification of germline, heterozygous mutations in the *PIK3CD* gene encoding p110δ in a cohort of fourteen patients from seven families with an unusual combination of lymphoproliferation and immunodeficiency.

Our patients presented usually in childhood with combined T and B cell immunodeficiency and peripheral expansion of lymphocytes. A major hallmark of this disease is the appearance of T and B cell$^+$ lymphoid nodules on respiratory and gastrointestinal mucosal surfaces, a phenotype that is of interest given data implicating PI(3)K and Akt in the regulation of T cell trafficking[40]. CD4$^+$ T cell counts were generally low, and profound defects in mitogen and antigen recall responses were observed. Common to all patients were EBV and/or CMV viremia (consistent with T cell defects) and recurrent sinopulmonary infections (consistent with humoral defects). The B cell abnormalities include accumulation of transitional B cells, paucity of memory B cells, and class switched immunoglobulin secretion defects, consistent with a role for PI(3)K in B cell development and maturation[41,42]. EBV$^+$ lymphoma was diagnosed in two patients, and an additional two individuals within our families died from lymphoma prior to our discovery of this genetic lesion. Genetic investigation of patients sharing this phenotype revealed GOF mutations in *PIK3CD*, the gene encoding p110δ. By structural comparison to p110α GOF mutations, we surmised that the E525K (helical domain) and the N334K (C2 domain) patient mutations were likely to disrupt specific inhibitory contacts between p110δ and the inter-SH2 (iSH2) and N-terminal SH2 (nSH2) domains of p85α, respectively[5,23,24,43]. In contrast, the E1021K patient p110δ mutation likely enhances recruitment to the plasma membrane and increases catalytic activity[22,23,25].

Given the EBV and CMV immunodeficiency, we focused our studies on CD8$^+$ T cells and unexpectedly found that total and virus-specific CD8$^+$ T cells were expanded with an enrichment in phenotypically “antigen-experienced” CD8$^+$ T cells. However, we observed

that patient CD8$^+$ T cells were severely impaired in *in vitro* proliferation and IL-2 secretion despite hyperphosphorylation of Akt. Akt activity is widely known to promote cell growth, proliferation, and metabolism, hence its major role in tumorigenesis[36]. Thus, we were initially surprised that hyperactivation of this pathway results in an immunodeficiency with a profound *in vitro* T proliferation and IL-2 production defect. Upon closer examination, we found that many aspects of TCR signaling are intact but T cells from patient blood are skewed toward senescent (CD57$^+$) and terminally differentiated T_{EMRA} or T_{EM} cells. As such, we hypothesized that the hyperactive p110δ-Akt-mTOR pathway was promoting aerobic glycolysis (the "Warburg effect"[7,8]), limiting the generation and survival of memory T cells[6,7,12,17], and driving CD8$^+$ T cell senescence[15,44]. Indeed, our patients exhibit p110δ- and mTOR-dependent hyperphosphorylation of S6 and increased glucose uptake in cultured T cell blasts, confirming that cell-intrinsic mTOR signaling is enhanced by the patient GOF mutations. Thus, over time, patients respond ineffectively to infections by inducing the terminal differentiation of CD8$^+$ T cells into senescent effectors without supporting the development of long-lived memory cells. Since it is widely accepted that memory T cells are critical for control of chronic infections, poor anti-EBV/CMV immunity in our patients is likely at least partially due to a reduced long-lived memory CD8$^+$ T cell pool[45]. Additionally, the mTOR-driven differentiation into effector cells could explain the lymphadenopathy since skewing toward effector-type cells may result in an enhanced proliferative burst upon encounter with antigen.

The above data provided the rationale for rapamycin therapy to inhibit mTOR, similar to interventions in specific cancers[46]. Although our experience with this intervention is limited at present, in patient A.1, rapamycin produced remarkable clinical improvement in lymphoproliferation and was associated with near normalization of peripheral T cell populations as well as better proliferation and IL-2 secretion by CD8$^+$ T cells *in vitro*. The restoration of naïve T cell populations supports our hypothesis that metabolic effects of mTOR play a central role in causing immunodeficiency. These findings raise the important clinical possibility that p110δ-specific inhibitors recently described[47] would also be effective in treating this disease and may, in fact, have improved efficacy over rapamycin since other, mTOR-independent pathways downstream of PI(3)K would also be targeted.

Although the possibility exists that chronic EBV and/or CMV infection contributes to appearance of CD57$^+$ CD8$^+$ T cells, we were unable to find a correlation between viral load and skewing of CD8$^+$ T cells. Our studies in another immunodeficiency with EBV, namely XMEN disease, have revealed that CD57 is expressed at normal levels on CD8$^+$ T cells despite viral loads higher than that seen in the disease described here (data not shown). We also noted that the most clinically affected patients (A.1 and G.1) also had signs of greatest mTOR activity (i.e., phosphorylation of S6 and glucose uptake). Moreover, treatment with rapamycin partially normalizes T cell populations, again supporting a cell-intrinsic, mTOR-driven mechanism of effector differentiation and senescence rather than effects of chronic viremia.

In conclusion, we have uncovered a novel human immunodeficiency we now term “PASLI Disease” for **p**110δ **A**ctivating mutation causing **S**enescent T cells, **L**ymphadenopathy, and **I**mmunodeficiency. PASLI Disease is caused by dominant, gain-of-function mutations in

PIK3CD that promote mTOR-mediated intrinsic $CD8^+$ T cell defects that, at least partially, explain the immune phenotype in these patients. These findings position p110δ as a critical player in regulation of human immunity.

METHODS

Human subjects and rapamycin therapy

All human subjects (or their guardians) in this study provided written informed consent in accordance with Helsinki principles for enrollment in research protocols (clinical trials registration number NCT00001355) that were approved by the Institutional Review Board of the National Institute of Allergy and Infectious Diseases, NIH. Blood from healthy donors was obtained at the NIH Clinical Center under approved protocols. Mutations will be automatically archived by Online Mendelian inheritance in Man (OMIM: 602839). We will also create a webpage through National Center for Biotechnology Information (NCBI) to accumulate patient mutation data in the format of the Leiden Online Variant Database (LOVD) as patients are identified. Patient A.1 was treated with once daily oral rapamycin at a dose of 1 mg, with initial calculation based on 1 mg/m^2, and subsequently adjusted to maintain a serum trough concentration of 12–15 ng/ml. All procedures were based on standard of care, and established clinical guidelines were followed.

Histology

Immunohistochemical stains were performed on formalin fixed paraffin embedded tissue biopsies using antibodies against EBV LMP1 (clone CS 1–4), IgG, and IgM (Dako). The stains were performed on an automated system (BenchMark, XT) according to the manufacturer's instructions. Images were taken using an Olympus B×41 microscope, objective UPlanFI 10×/030 and 20×/0.50 ∞/0.17, with an adaptor U-TV0.5×C using a digital camera Q-imaging Micropublisher 5.0 RTV. The images were captured using "Q-Capture Version 3.1" and imported into Adobe Photoshop 7.0.

DNA sequencing

Genomic DNA was submitted to Otogenetics for whole exome capture [Agilent V4 (51 Mbp)] and next-generation sequencing on the Illumina HiSSeq2000. Next-generation sequencing results were confirmed by Sanger sequencing. *PIK3CD* coding exons were PCR-amplified using exon specific oligonucleotide primers and GoTaq Hot Start Polymerase (Promega) (primer sequences and cycling conditions are provided in Supplementary Table 2). Purified PCR products were directly sequenced using BigDye Terminators (version 1.1) and analyzed on a 3130×L Genetic Analyzer (Applied Biosystems).

Bioinformatics

The DNAnexus interface was used to align the Illumina reads to the hg19 human reference genome and perform SNP and INDEL discovery and genotyping. To prioritize the variant calls, we implemented the ANNOVAR functional annotation package, filtering the output based on gene/amino acid annotation, functional prediction scores, nucleotide conservation scores, and allele frequencies per the NCBI dbSNP database (build 137), The 1000 Genomes Project (2012 April release), and the NHLBI GO Exome Sequencing Project (ESP6500).

Only non-synonymous novel variants or variants with population frequencies less than 1% were considered further. All candidates were predicted to be damaging by the SIFT, PP2, LRT, MutationTaster, and MutationAssessor tools. Exomic variants were finally prioritized based on clinical correlation and protein structure analysis.

Protein structure analysis

Multiple protein sequence alignment of p110δ catalytic subunits was carried out using Clustal Omega[48]. As no experimentally derived structural data for p110δ have been reported, we mapped the corresponding positions of the patients' p110δ mutations onto a structural homolog, human p110α (PDB ID: 3HHM). Due to the high sequence homology between p110δ and p110α (39% amino acid identity and 72% amino acid identity +similarity; Supplementary Fig. 3), the p110δ mutation positions could be confidently determined on the p110α structure. Importantly, the reference structure 3HHM contains both the p110α catalytic subunit and the p85α regulatory component of the PI(3)K complex, allowing us to compare the position of the mutations relative to critical membrane contacts that arise from recruitment by p85α.

Cell culture and transfection

Human PBMCs were isolated by Ficoll-Paque PLUS (GE Healthcare) density gradient centrifugation, washed twice in phosphate buffered saline (PBS), and resuspended at 10^6 cells/ml complete RPMI-1640 (cRPMI) medium (Lonza) containing 10% fetal bovine serum (FBS), 2 mM glutamine, and penicillin and streptomycin (100 U/ml each, Invitrogen). Cells were activated with 1 μg/ml anti-CD3 (clone HIT3α, BD Biosciences) and 1 μg/ml anti-CD28 (clone CD28.2, BD Biosciences) in the presence of 100 IU/ml human IL-2. After 3 days, activated T cells were washed and then cultured in cRPMI medium supplemented with 100 U/ml recombinant human IL-2 (rhIL-2, R&D). Activated T cell subsets were separated using CD4 or CD8 microbeads (Miltenyi Biotech). The mouse mastocytoma cell line P815 (ATCC) and the human H9 T cell line (ATCC) were maintained in cRPMI. Transfection was performed with Amaxa Nucleofection kits (Lonza) for primary cells and with standard electroporation for cell lines. For CTL studies in Fig. 3, human PBMCs were stimulated with irradiated allogeneic buffy coats in the presence of 1 μg/ml phytohaemagglutinin (PHA), and cultured in cRPMI medium containing 5% human AB serum (Sigma), 2 mM L-glutamine, 1 mM sodium pyruvate, 1 mM sodium bicarbonate, 50 μM β-mercaptoethanol, 100 U/ml penicillin, 100 μg/ml streptomycin, and 100 U/ml rhIL-2. Activated $CD4^+$ and $CD8^+$ T cells were purified by negative selection using microbeads (Miltenyi Biotech).

Flow cytometry

For standard surface staining, PBMCs (1×10^6 cells per sample), sorted cells, expanded T cells, or cell lines were washed with PBS and incubated for 30 min at 4 °C (dark) in 100 μl 5% FBS in PBS with indicated fluorochrome-labeled monoclonal antibodies or their isotype controls. After washing with PBS two times, $1–5 \times 10^4$ live cells were analyzed by flow cytometry. Validated antibodies against CD20, CD27, CD10, CD5, IgG, IgA, CD3, CD4, CD8, CCR7, CD62L, CD45RA, IFN-γ, T-bet, granzyme B, LAMP-1, CD57, CD38, and PD-1 were purchased from BD Biosciences, eBioscience, or BioLegend. For phosflow staining, unless otherwise indicated, cells were kept in cRPMI while alive, fixed directly in

cRPMI using BD Lyse-Fix, and then permeabilized with BD perm buffer III according to manufacturer's instructions. For phosflow analyses, anti-pAkt S473 Alexa Fluor 647 (Cell Signaling, D9E), anti-pAkt T308 Alexa Fluor 488 (Cell Signaling, C31E5E), anti-pS6 S235, S236 PE (BD Biosciences, N7-548), and anti-pS6 S240, S244 Alexa Fluor 647 (Cell Signaling, D68F8) were used.

Tetramer staining

As previously described[49], MHC class I tetramers were purchased from Immudex or Proimmune. CMV epitopes used were the HLA-A* 0201-restricted peptides NLVPMVATV from pp65 (UL83) protein, and VTEHDTLLY from pp50 (UL44) protein. EBV epitopes used were HLA-A*0201-restricted GLCTLVAML from the lytic Ag BMLF-1, CLGGLLTMV from latent antigen LMP2, HLA-B*0801-restricted peptides RAKFKQLL from BZLF1 lytic protein and FLRGRAYGL from latent protein EBNA3A.

Proliferation assays

CFSE dilution: PBMCs, either freshly isolated or thawed from liquid nitrogen–stored samples, were incubated with CellTrace CFSE Cell Proliferation Kit (1 μM; Invitrogen). After 5 min, cells were washed twice with cRPMI. A total of 1×10^5 cells were seeded into 96-well plates, stimulated with CD3/CD28 (Dynabeads T-cell activator from Invitrogen), or PHA (1 μg/ml; Sigma-Aldrich) with or without IL-2 (100 units/ml) as indicated in the figures. After 72 h cells were stained with CD4-APC and CD8-PerCP for 30 min at 4 °C (dark), washed with PBS twice, and 1×10^4 live cells were analyzed by flow cytometry (Becton Dickinson FACSCanto II). Thymidine incorporation was assessed either three days (mitogens) or six days (antigens) after stimulation in accordance with established guidelines.

Cytokine measurements

PBMCs (1×10^6/ml) were stimulated with Dynabeads T cell activator CD3/CD28 for 24–72 h as indicated in the figure. Cell-free supernatants were harvested and cytokines were measured simultaneously with Fluorokine MAP Human Base Kit A (R&D Systems) using the Luminex 200 System (Luminex Corporation). For intracellular cytokine staining, activated T cells were restimulated with plate-bound anti-CD3 (clone OKT3, 1 μg/ml) or PMA plus Ionomycin for 6 h in the presence of monensin. Cells were then washed in medium, fixed and permeabilized using BD Cytofix/Cytoperm Buffer and stained intracellularly with antibodies against cytokines of interest.

B cell studies

Human B cell subsets were phenotyped by flow cytometry and naive and memory B cells sorted and cultured *in vitro* to asses proliferation, class switching to IgG, induction of *AICDA* expression and Ig secretion as previously described[50].

Immunoblotting

Cells were washed in PBS or RPMI with no FCS and immediately lysed in 1% Triton X-100, 50 mM Tris-HCl pH 8, 150 mM NaCl, 2 mM EDTA, 10% glycerol, complete protease inhibitor cocktail (Roche), and phosphatase inhibitor cocktails (Sigma). Protein was

quantitated by BCA assay (Pierce). The lysates were then clarified by centrifugation at 15,000 × g at 4 °C for 10 min. Supernatants were transferred to a separate tube and used for subsequent experimentation. Approximately 20 μg total protein was separated by SDS-PAGE and transferred to a nitrocellulose membrane (Bio-Rad). Membranes were blocked with 5% non-fat dry milk in Tris-buffered saline (TBS) pH 8.5 with 0.01% Tween-20 (TBST) for 1 h at 21°C before incubating with primary antibody overnight at 4 °C. After washing with TBST for 1 h at 21°C, HRP-conjugated secondary antibody was added for an additional hour at 21°C. Following a final 1 h wash step, HRP substrate (Luminata Forte, Millipore) was added to the membranes, which were then subjected to chemiluminscent imaging. Validated primary antibodies were purchased from Cell Signaling Technology or Santa Cruz Biotechnology, and secondary antibodies were from Southern Biotech. Band intensities were quantified using ImageJ. Antibodies were against: p110δ (Millipore 04–401), p-Akt (S473) (Cell Signaling 4060), Akt (Cell Signaling 4691), β-tubulin (Cell Signaling 2128), Flag (Sigma M2), PTEN (Cell Signaling 9188), PKCθ (Santa Cruz sc-212), p-Erk (Cell Signaling 4370), Erk (Cell Signaling 4695), ARF6 (Cell Signaling 5740), and p27kip1 (Cell Signaling 3686).

Degranulation and cytolysis assays

Activated T cells were stimulated with plate-bound antibodies against CD3 (1 μg/ml), previously blocked with 10% FBS, in the presence of PE-conjugated anti-LAMP1 (H4A3) for 2 h or 4 h at 37 °C. Cells were then washed and stained for surface expression of LAMP1, and analyzed by flow cytometry. To assess general cytolytic activity, P815 cells presenting anti-CD3 were used as targets in a redirected cytotoxicity assay. Cytolytic activity was assayed *in vitro* by measuring the release of lactate dehydrogenase (LDH) from target cells using the Cytotox96 cytotoxicity assay (Promega) following manufacturer's instructions.

Calcium flux assessment

Activated T cell blasts were loaded with 1 μM Fluo4 and 2 μM FuraRed (Molecular Probes) in Powerload (Molecular Probes) for 15 min at 37 °C before being washed with PBS and resuspended in Hank's Balanced Salt Solution buffer containing 1.5 mM $CaCl_2$ and 1.5 mM $MgCl_2$. Flux was assessed by flow cytometry upon stimulation with anti-CD3 (clone HIT3α, BD Biosciences) plus Protein A (Sigma).

Confocal imaging

Cells were stimulated with anti-CD3 (clone HIT3α, BD Biosciences), dropped on poly-L-lysine-coated slides (Electron Microscopy Sciences), and fixed with 3% paraformaldehyde in PBS before permeabilizing with 0.05% Triton X-100 for 3–5 min at 21°C and blocking with 0.5% BSA in PBS. Stains and washes were with 0.5% BSA in PBS using anti-p65 NF-κB (Santa Cruz sc-372). Slides were mounted with Fluoromount-G with DAPI (Southern Biotech) and visualized with a Leica SP5 confocal microscope (Carl Zeiss) with a 63× magnification objective, and micrographs were analyzed using Imaris 7.4.2 (Bitplane Scientific Software).

Glucose Uptake

Cells were starved of glucose by incubation in PBS for 1 h prior to incubation with 100 μg/mL 2-deoxy-2-[(7-nitro-2,1,3-benzoxadiazol-4-yl)amino]-D-glucose (2-NBDG) (Cayman Chemical) for 20 min. Uptake was measured by flow cytometric evaluation of signal in the fluorescein channel collected in log (Fig. 4f) or linear (Supplementary Fig. 8c) mode.

Statistical analyses

Data were analyzed using Student's *t*-test (paired or unpaired, using Welch's correction when standard deviation in the groups were unequal) or non-parametric Mann-Whitney U test (when data do not follow a normal distribution) as indicated utilizing the Prism (Graph Pad) software. Only when a value was greater than two standard deviations from the mean was it excluded from analysis. Whenever possible, at least 3 patients and 3 normal controls were examined for each analysis to enable sufficient statistical power.

Supplementary Material

Refer to Web version on PubMed Central for supplementary material.

Acknowledgments

The authors thank the referring physicians as well as our patients and families who have gone to extraordinary efforts to join this study and provided samples. This research was supported by the Division of Intramural Research, National Institute of Allergy and Infectious Diseases, Clinical Center, and National Human Genome Research Institute, National Institutes of Health. This project has been funded in whole or in part with federal funds from the Frederick National Laboratory for Cancer Research, National Institutes of Health, under Contract No. HHSN261200800001E. Parts of this work were funded by project and program grants from the National Health and Medical Research Council (NHMRC) of Australia (to E.K.D., U.P., S.G.T.), the Cancer Council NSW (to S.G.T.) and the Cancer Institute NSW (to U.P.). S.G.T. is a recipient of a Principal Research Fellowship from the NHMRC of Australia. L.M. is the recipient of a Postdoctoral Fellowship from the Research Foundation-Flanders (FWO), Belgium. C.L.L. was supported by the Postdoctoral Research Associate (PRAT) Fellowship and R.Z. supported by the Medical Scientist Training Program through the National Institute of General Medical Sciences. The content of this publication does not necessarily reflect the views or policies of the Department of Health and Human Services, nor does mention of trade names, commercial products, or organizations imply endorsement by the U.S. Government.

References

1. Okkenhaug K, Vanhaesebroeck B. PI3K in lymphocyte development, differentiation and activation. Nat. Rev. Immunol. 2003; 3:317–330. [PubMed: 12669022]
2. Hemmings BA, Restuccia DF. PI3K-PKB/Akt pathway. Cold Spring Harb Perspect Biol. 2012; 4:a011189. [PubMed: 22952397]
3. Chantry D, et al. p110delta, a novel phosphatidylinositol 3-kinase catalytic subunit that associates with p85 and is expressed predominantly in leukocytes. J. Biol. Chem. 1997; 272:19236–19241. [PubMed: 9235916]
4. Vanhaesebroeck B, et al. P110delta, a novel phosphoinositide 3-kinase in leukocytes. Proc Natl Acad Sci USA. 1997; 94:4330–4335. [PubMed: 9113989]
5. Huang CH, et al. The structure of a human p110alpha/p85alpha complex elucidates the effects of oncogenic PI3Kalpha mutations. Science. 2007; 318:1744–1748. [PubMed: 18079394]
6. Gubser PM, et al. Rapid effector function of memory CD8 T cells requires an immediate-early glycolytic switch. Nat Immunol. 2013; 14:1064–1072. [PubMed: 23955661]

7. Xu X, Ye L, Araki K, Ahmed R. mTOR, linking metabolism and immunity. Semin Immunol. 2012; 24:429–435. [PubMed: 23352227]
8. Yang K, Chi H. mTOR and metabolic pathways in T cell quiescence and functional activation. Semin Immunol. 2012; 24:421–428. [PubMed: 23375549]
9. Zinzalla V, Stracka D, Oppliger W, Hall MN. Activation of mTORC2 by association with the ribosome. Cell. 2011; 144:757–768. [PubMed: 21376236]
10. Alessi DR, et al. Characterization of a 3-phosphoinositide-dependent protein kinase which phosphorylates and activates protein kinase Balpha. Curr Biol. 1997; 7:261–269. [PubMed: 9094314]
11. Sarbassov DD, Guertin DA, Ali SM, Sabatini DM. Phosphorylation and regulation of Akt/PKB by the rictor-mTOR complex. Science. 2005; 307:1098–1101. [PubMed: 15718470]
12. Kaech SM, Cui W. Transcriptional control of effector and memory CD8+ T cell differentiation. Nat Rev Immunol. 2012; 12:749–761. [PubMed: 23080391]
13. Finlay DK, et al. PDK1 regulation of mTOR and hypoxia-inducible factor 1 integrate metabolism and migration of CD8+ T cells. J Exp Med. 2012; 209:2441–2453. [PubMed: 23183047]
14. Fox CJ, Hammerman PS, Thompson CB. Fuel feeds function: energy metabolism and the T-cell response. Nat Rev Immunol. 2005; 5:844–852. [PubMed: 16239903]
15. Astle MV, et al. AKT induces senescence in human cells via mTORC1 and p53 in the absence of DNA damage: implications for targeting mTOR during malignancy. Oncogene. 2012; 31:1949–1962. [PubMed: 21909130]
16. Kim EH, Suresh M. Role of PI3K/Akt signaling in memory CD8 T cell differentiation. Front Immunol. 2013; 4:20. [PubMed: 23378844]
17. Araki K, et al. mTOR regulates memory CD8 T-cell differentiation. Nature. 2009; 460:108–112. [PubMed: 19543266]
18. Kim EH, et al. Signal integration by Akt regulates CD8 T cell effector and memory differentiation. J Immunol. 2012; 188:4305–4314. [PubMed: 22467649]
19. Sukumar M, et al. Inhibiting glycolytic metabolism enhances CD8+ T cell memory and antitumor function. Journal of clinical investigation. 2013; 123:4479–4488. [PubMed: 24091329]
20. Jarrett AF, Armstrong AA, Alexander E. Epidemiology of EBV and Hodgkin's lymphoma. Ann Oncol. 1996; 4(7 Suppl):5–10. [PubMed: 8836402]
21. Berndt A, et al. The p110delta structure: mechanisms for selectivity and potency of new PI(3)K inhibitors. Nat Chem Biol. 2010; 6:117–124. [PubMed: 20081827]
22. Bader AG, Kang S, Zhao L, Vogt PK. Oncogenic PI3K deregulates transcription and translation. Nat Rev Cancer. 2005; 5:921–929. [PubMed: 16341083]
23. Mandelker D, et al. A frequent kinase domain mutation that changes the interaction between PI3Kalpha and the membrane. Proc Natl Acad Sci U S A. 2009; 106:16996–17001. [PubMed: 19805105]
24. Wu H, et al. Regulation of Class IA PI 3-kinases: C2 domain-iSH2 domain contacts inhibit p85/p110alpha and are disrupted in oncogenic p85 mutants. Proc Natl Acad Sci U S A. 2009; 106:20258–20263. [PubMed: 19915146]
25. Zhao L, Vogt PK. Helical domain and kinase domain mutations in p110alpha of phosphatidylinositol 3-kinase induce gain of function by different mechanisms. Proc Natl Acad Sci U S A. 2008; 105:2652–2657. [PubMed: 18268322]
26. Jou ST, et al. Identification of variations in the human phosphoinositide 3-kinase p110delta gene in children with primary B-cell immunodeficiency of unknown aetiology. Int J Immunogenet. 2006; 33:361–369. [PubMed: 16984281]
27. Damgaard RB, et al. Disease-causing mutations in the XIAP BIR2 domain impair NOD2-dependent immune signalling. EMBO Mol Med. 2013; 5:1278–1295. [PubMed: 23818254]
28. Li FY, et al. Second messenger role for Mg2+ revealed by human T-cell immunodeficiency. Nature. 2011; 475:471–476. [PubMed: 21796205]
29. Brenchley JM, et al. Expression of CD57 defines replicative senescence and antigen-induced apoptotic death of CD8+ T cells. Blood. 2003; 101:2711–2720. [PubMed: 12433688]

30. Roux PP, et al. RAS/ERK signaling promotes site-specific ribosomal protein S6 phosphorylation via RSK and stimulates cap-dependent translation. J Biol Chem. 2007; 282:14056–14064. [PubMed: 17360704]
31. Okkenhaug K, et al. Impaired B and T cell antigen receptor signaling in p110delta PI 3-kinase mutant mice. Science. 2002; 297:1031–1034. [PubMed: 12130661]
32. Fruman DA, et al. Impaired B cell development and proliferation in absence of phosphoinositide 3-kinase p85alpha. Science. 1999; 283:393–397. [PubMed: 9888855]
33. Suzuki H, et al. Xid-like immunodeficiency in mice with disruption of the p85alpha subunit of phosphoinositide 3-kinase. Science. 1999; 283:390–392. [PubMed: 9888854]
34. Conley ME, et al. Agammaglobulinemia and absent B lineage cells in a patient lacking the p85alpha subunit of PI3K. J Exp Med. 2012; 209:463–470. [PubMed: 22351933]
35. Suzuki A, et al. T cell-specific loss of Pten leads to defects in central and peripheral tolerance. Immunity. 2001; 14:523–534. [PubMed: 11371355]
36. Denley A, Kang S, Karst U, Vogt PK. Oncogenic signaling of class I PI3K isoforms. Oncogene. 2008; 27:2561–2574. [PubMed: 17998941]
37. Zhao L, Vogt PK. Class I PI3K in oncogenic cellular transformation. Oncogene. 2008; 27:5486–5496. [PubMed: 18794883]
38. Vivanco I, Sawyers CL. The phosphatidylinositol 3-Kinase AKT pathway in human cancer. Nat Rev Cancer. 2002; 2:489–501. [PubMed: 12094235]
39. Billottet C, et al. A selective inhibitor of the p110delta isoform of PI 3-kinase inhibits AML cell proliferation and survival and increases the cytotoxic effects of VP16. Oncogene. 2006; 25:6648–6659. [PubMed: 16702948]
40. Sinclair LV, et al. Phosphatidylinositol-3-OH kinase and nutrient-sensing mTOR pathways control T lymphocyte trafficking. Nat Immunol. 2008; 9:513–521. [PubMed: 18391955]
41. Omori SA, et al. Regulation of class-switch recombination and plasma cell differentiation by phosphatidylinositol 3-kinase signaling. Immunity. 2006; 25:545–557. [PubMed: 17000121]
42. Srinivasan L, et al. PI3 kinase signals BCR-dependent mature B cell survival. Cell. 2009; 139:573–586. [PubMed: 19879843]
43. Amzel LM, et al. Structural comparisons of class I phosphoinositide 3-kinases. Nat Rev Cancer. 2008; 8:665–669. [PubMed: 18633356]
44. Yentrapalli R, et al. The PI3K/Akt/mTOR Pathway Is Implicated in the Premature Senescence of Primary Human Endothelial Cells Exposed to Chronic Radiation. PLoS One. 2013; 8:e70024. [PubMed: 23936371]
45. Gourley TS, Wherry EJ, Masopust D, Ahmed R. Generation and maintenance of immunological memory. Semin Immunol. 2004; 16:323–333. [PubMed: 15528077]
46. Faivre S, Kroemer G, Raymond E. Current development of mTOR inhibitors as anticancer agents. Nat Rev Drug Discov. 2006; 5:671–688. [PubMed: 16883305]
47. Lannutti BJ, et al. CAL-101, a p110delta selective phosphatidylinositol-3-kinase inhibitor for the treatment of B-cell malignancies, inhibits PI3K signaling and cellular viability. Blood. 2011; 117:591–594. [PubMed: 20959606]
48. Sievers F, et al. Fast, scalable generation of high-quality protein multiple sequence alignments using Clustal Omega. Mol Syst Biol. 2011; 7:539. [PubMed: 21988835]
49. Palendira U, et al. Molecular pathogenesis of EBV susceptibility in XLP as revealed by analysis of female carriers with heterozygous expression of SAP. PLoS Biol. 2011; 9:e1001187. [PubMed: 22069374]
50. Avery DT, et al. B cell-intrinsic signaling through IL-21 receptor and STAT3 is required for establishing long-lived antibody responses in humans. J Exp Med. 2010; 207:155–171. [PubMed: 20048285]

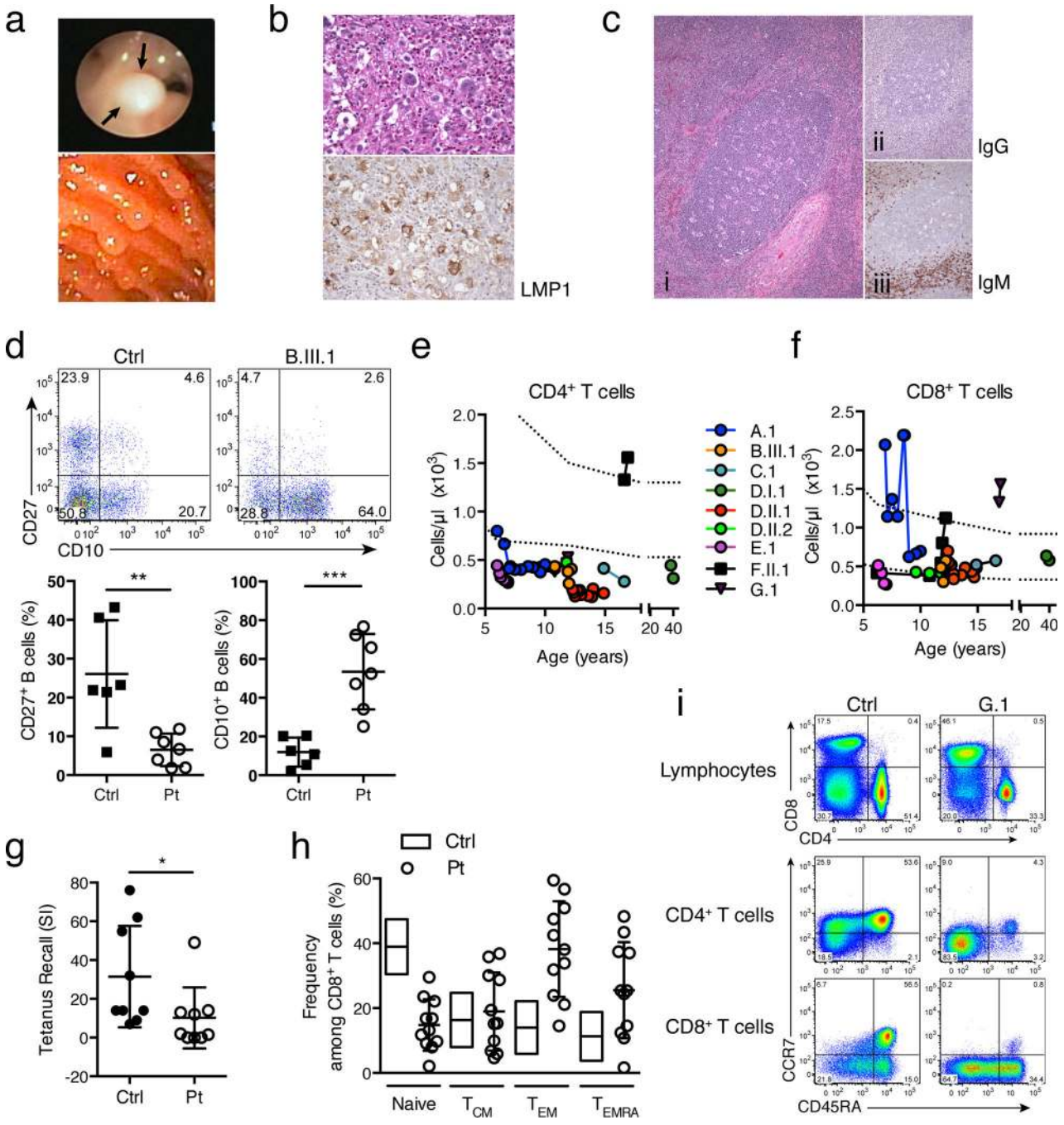

Figure 1. A novel primary immunodeficiency characterized by T and B cell accumulation with lymphoid nodules and defective memory cell populations

(a) Endoscopic imaging reveals nodules in airways (top, patient E.1) and gastrointestinal tract (bottom, patient A.1) with lymphocytic infiltrates. Data are representative of 6 patients examined. **(b)** H & E staining of histological sections of a lymphoma biopsy from patient F.II.1 reveals a nodular sclerosis form of classical Hodgkin lymphoma (top); LMP-1 stain revealed EBV latent membrane antigen (brown coloration, 3,3'-Diaminobenzidine) (bottom). **(c)** Hematoxylin and eosin (H & E) staining (i) and immunoperoxidase staining

for IgG (ii) and IgM (iii) on histological sections of lymph node from patient G.1. **(d)** The proportion (numbers in quadrants are percentages) of transitional ($CD10^+CD27^-$), naïve ($CD10^-CD27^-$) and memory ($CD10^-CD27^+$) cells within the B-cell population of a healthy control (Ctrl, top left) or patient B.III.1 (top right). Representative of 4 independent experiments. Each symbol in the bottom graphs shows cumulative data for memory (bottom left, $P = 0.004$ by two-tailed, unpaired *t*-test) and transitional (bottom right, $P = 0.0005$ by two-tailed, unpaired *t*-test) B cells represents an individual healthy control (Ctrl, $n = 6$) or patient (Pt, $n = 7$), and the horizontal bars represent means. Peripheral blood $CD4^+$ T cell counts **(e)** and $CD8^+$ T cell counts **(f)** in indicated patients as a function of age in years over time in all nine patients. **(g)** Thymidine incorporation assay for proliferation in response to the tetanus recall antigen, comparing normal controls ($n = 9$) and patients ($n = 9$) and showing mean and standard deviation as horizontal lines. Data are cumulative from 9 independent experiments. SI = stimulation index of the value with antigen divided by that with no antigen. $P = 0.01$ by Mann-Whitney test. **(h)** Composite graph showing T_{naive} ($CD45RA^+CD62L^+$), T_{CM} ($CD45RA^-CD62L^+$), T_{EM} ($CD45RA^-CD62L^-$), and T_{EMRA} ($CD45RA^+CD62L^-$) populations among $CD8^+$ T cells in all living patients (Pt, $n = 11$) compared to the clinical normal range derived from 50 healthy controls (Ctrl). **(i)** Representative flow cytometric dot plots of PBMCs from patient G.1 or a health control (Ctrl) stained for $CD8^+$ versus $CD4^+$ T cells (gated on lymphocytes, top) or CCR7 versus CD45RA gated on $CD4^+$ (middle) or $CD8^+$ (bottom) lymphocytes, showing T_{naive} ($CD45RA^+CCR7^+$), T_{CM} ($CD45RA^-CCR7^+$), T_{EM} ($CD45RA^-CCR7^-$), and T_{EMRA} ($CD45RA^+CCR7^-$) populations. Events falling into each quadrant are given as a percentage of the total. Data are representative of 5 independent experiments on multiple patients (see Supplementary Fig. 1D).

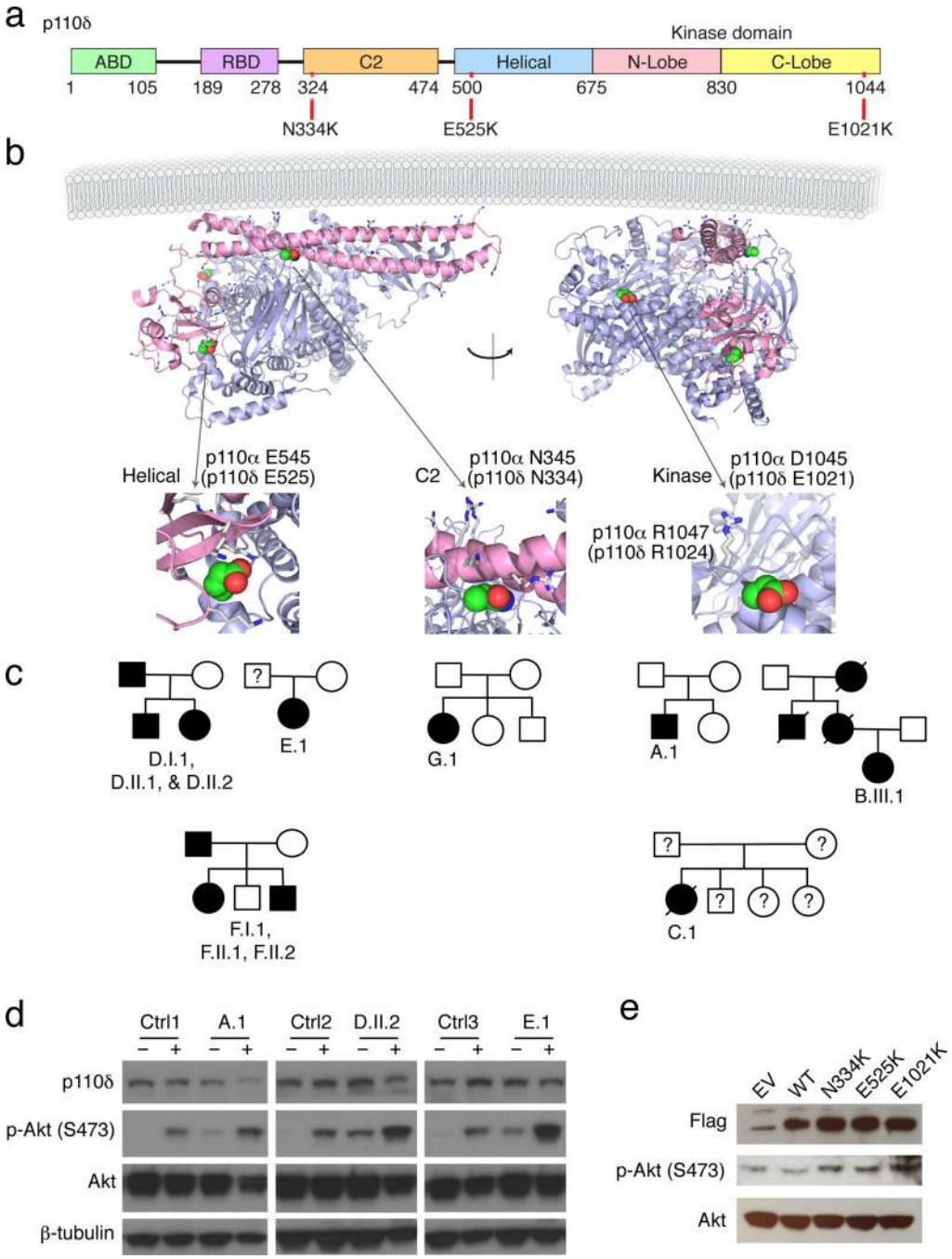

Figure 2. Heterozygous, gain-of-function mutation in PIK3CD in all affected individuals causes AKT hyperphosphorylation

(a) Schematic of p110δ protein domains (as described in the text) with patient mutations labeled with red lines. **(b)** Location of patient mutations (green spheres) shown on the structure (PDB 3HHM) of human p110α H1047R mutant (blue) in complex with p85α (pink). Positively charged amino acids along the membrane-binding face of p110 are shown as grey sticks. Location of the p110αH1047R mutation indicated by grey sticks. **(c)** Pedigrees of affected families with mutation-positive (black), unaffected (white), unscreened

(grey), and deceased (diagonal) individuals. **(d)** Immunoblot on serum-starved, activated T cells using antibodies for p110δ, Akt, p-Akt (S473), and β-tubulin as indicated for patients D.II.1, D.II.2, and E.1 compared to three normal controls (Ctrl) with 10 min anti-CD3 stimulation (+) or not (−). Data are quantified in Supplementary Fig. 4A and are representative of p-Akt (S473) results from 4 independent experiments. **(e)** Immunoblot for Flag, p-Akt (S473), and total Akt on lysates from unactivated healthy control PBMCs overexpressing empty vector (EV), WT p110δ, or mutant p110δ 16 hr post-transfection. Data are representative of 3 independent experiments that were quantified in Supplementary Fig. 4F.

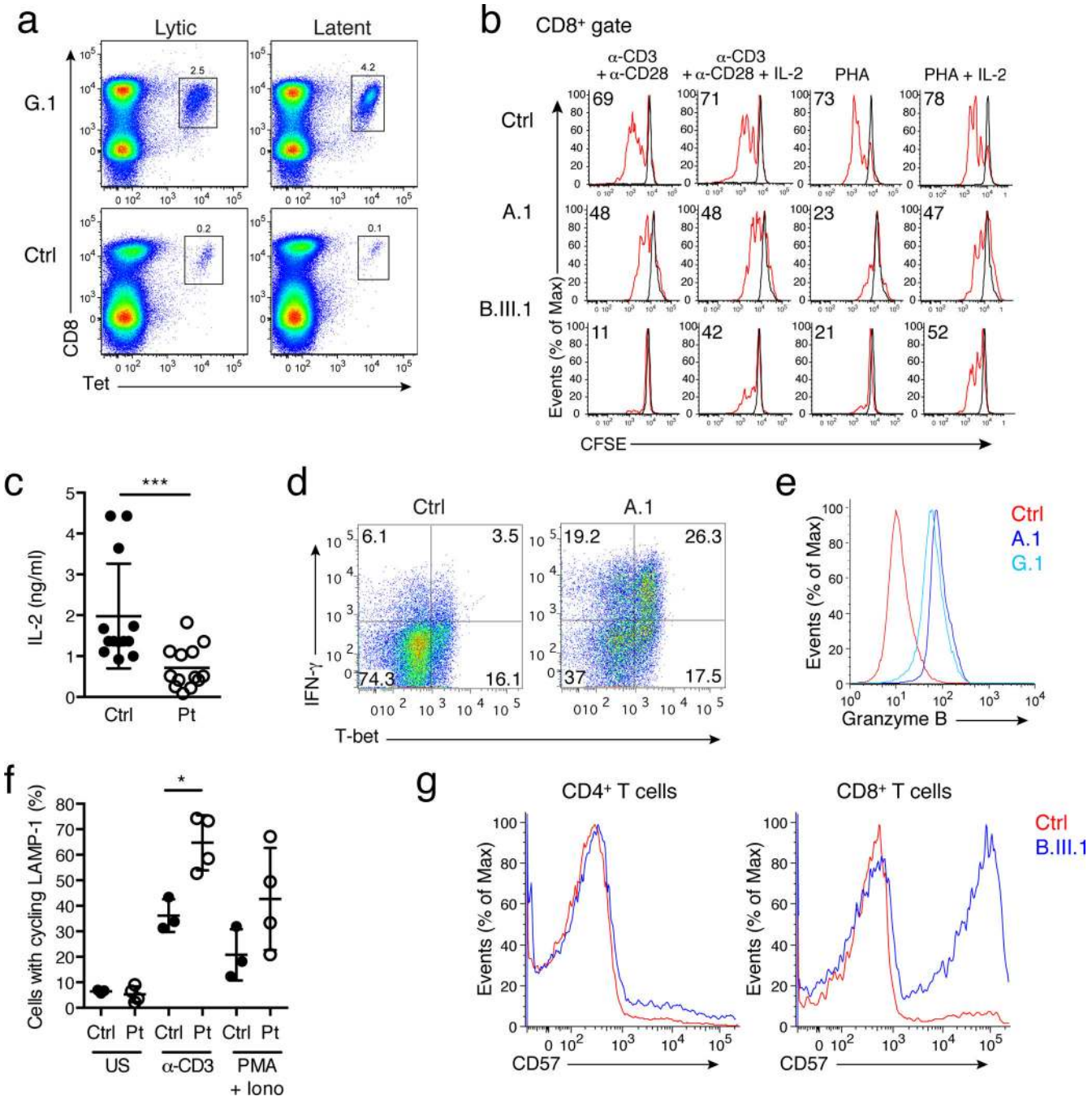

Figure 3. Patient PBMCs contain virus-specific CD8 T cells but fail to proliferate upon TCR stimulation in vitro due to terminal differentiation and senescence

(a) Flow cytometry analysis of EBV-specific tetramer staining of patient G.1 and control PBMCs for detection of EBV lytic and latent antigen-specific CD8$^+$ T cells. Numbers in quadrants represent the percentage of total. Data are representative of 4 independent experiments. **(b)** CFSE dilution on gated CD8$^+$ T cells for patients A.1 or B.III.1 compared to control 72 hrs after stimulation of PBMCs with the indicated mitogen. PHA = phytohemagglutinin. The percentage of cells that have divided is indicated. Data are

representative of 8 patients examined in 6 independent experiments. **(c)** IL-2 secretion 48–72 hrs after activation of PBMCs from normals ($n = 13$ from combined experiments) and patients ($n = 13$ from combined experiments) with anti-CD3/CD28 Dynabeads. Horizontal line indicates mean value, and $P = 0.0006$ by Mann Whitney test. Data are representative of 4 independent experiments. **(d)** Intracellular flow cytometry for IFN-γ production and T-bet expression in activated $CD8^+$ T cells stimulated with low-dose, immobilized anti-CD3. Numbers in quadrants represent the percentage of total. Data are quantified in Supplementary Fig. 5D and are representative of 3 independent experiments. **(e)** Granzyme B expression in activated $CD8^+$ T cells from patients A.1 and G.1 compared to control. Combined data from independent experiments are quantified in Supplementary Fig. 5E. **(f)** Flow cytometric measurement of LAMP-1 cycling in unstimulated (US) or stimulated (as indicated) $CD8^+$ T cells from patients (Pt, $n = 4$) compared to healthy controls (Ctrl, $n = 3$). Patients include A.1, E.1, F.II.1, and G.1. Horizontal line indicates mean value, and $P = 0.01$ obtained using the unpaired, two-tailed *t*-test. Data are representative of 3 independent experiments. **(g)** CD57 expression on $CD4^+$ (left) or $CD8^+$ (right) T cells from patient B.III. 1 compared to healthy control (Ctrl). Data are representative of 4 patients examined in 3 independent experiments, which are quantified in Supplementary Fig. 5H.

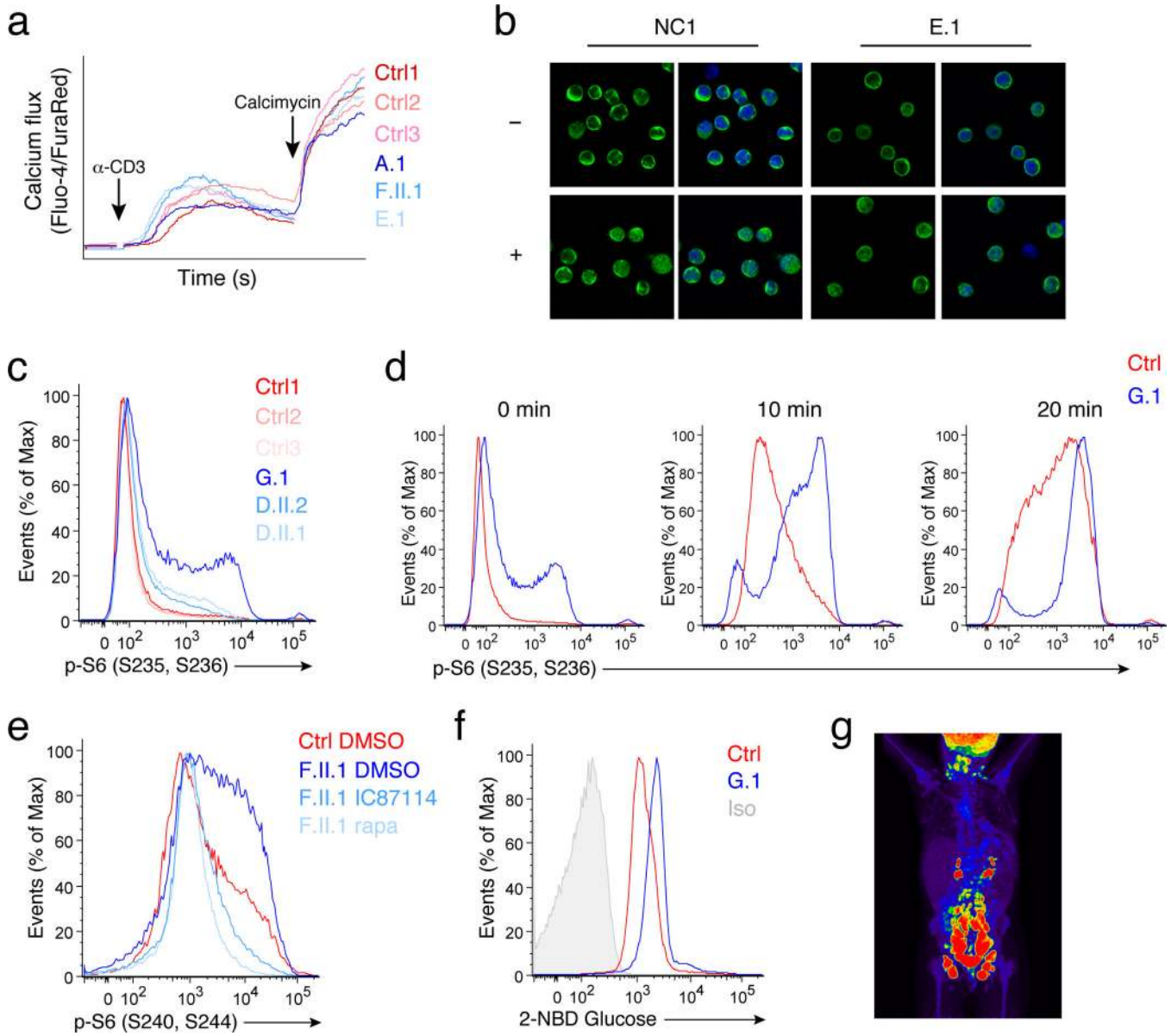

Figure 4. Patient T cells exhibit normal TCR signaling responses but elevated mTOR activity and glucose uptake in vitro

(a) Calcium flux (as measured by the ratio of Fluo-4 to FuraRed) induced by anti-CD3 stimulation in T cell blasts from patients A.1, E.1, and F.II.1 compared to controls. The calcimycin ionophore shows is used as a positive control. Data are representative of 2 independent experiments examining cells from 5 different patients. **(b)** Confocal microscopy showing NF-κB p65 (green, left panels) translocation into the nucleus stained by 4',6-Diamidino-2-Phenylindole, Dihydrochloride (DAPI, blue, colors merged right panels) in serum-starved T cell blasts following TCR stimulation (+) or not (−). Data are representative of 3 patients examined. **(c)** Phosflow analysis for phosphorylation of S6 (at residues S235 and S236) in unstimulated T cell blasts (fixed in complete medium) from patients G.1, D.II. 1, and D.II.2 compared to controls. Data are representative of 3 independent experiments and are quantified in Supplementary Fig. 8A. **(d)** Phosflow analysis of S6 phosphorylation at

S235, S236 at baseline (0 min) and 10 min or 20 min after stimulation with anti-CD3 plus protein A for patient G.1 (blue) and a healthy control (red). Data are representative of 2 independent experiments. **(e)** Phosflow analysis of S6 phosphorylation at residues S240 and S244 in unstimulated T cell blasts from patient F.II.1 treated for 20 min with DMSO, 10 μM IC87114 (p110δ inhibitor), or 50 nM rapamycin (mTOR inhibitor) compared to healthy control (Ctrl). Data are representative of 3 independent experiments. **(f)** Glucose uptake measured by flow cytometry analysis of the fluorescent deoxyglucose analog 2-NBDG in glucose-starved T cell blasts from patient G.1 compared to control (Ctrl). Data are representative of 4 experiments with a quantified analysis shown in Supplementary Fig. 8C. **(g)** Positron Emission Tomography (PET) scan of patient G.1 following administration of 18F-fludeoxyglucose analog shows glucose uptake most pronounced in the iliac chains and inguinal regions bilaterally. Data are representative of 3 patients examined.

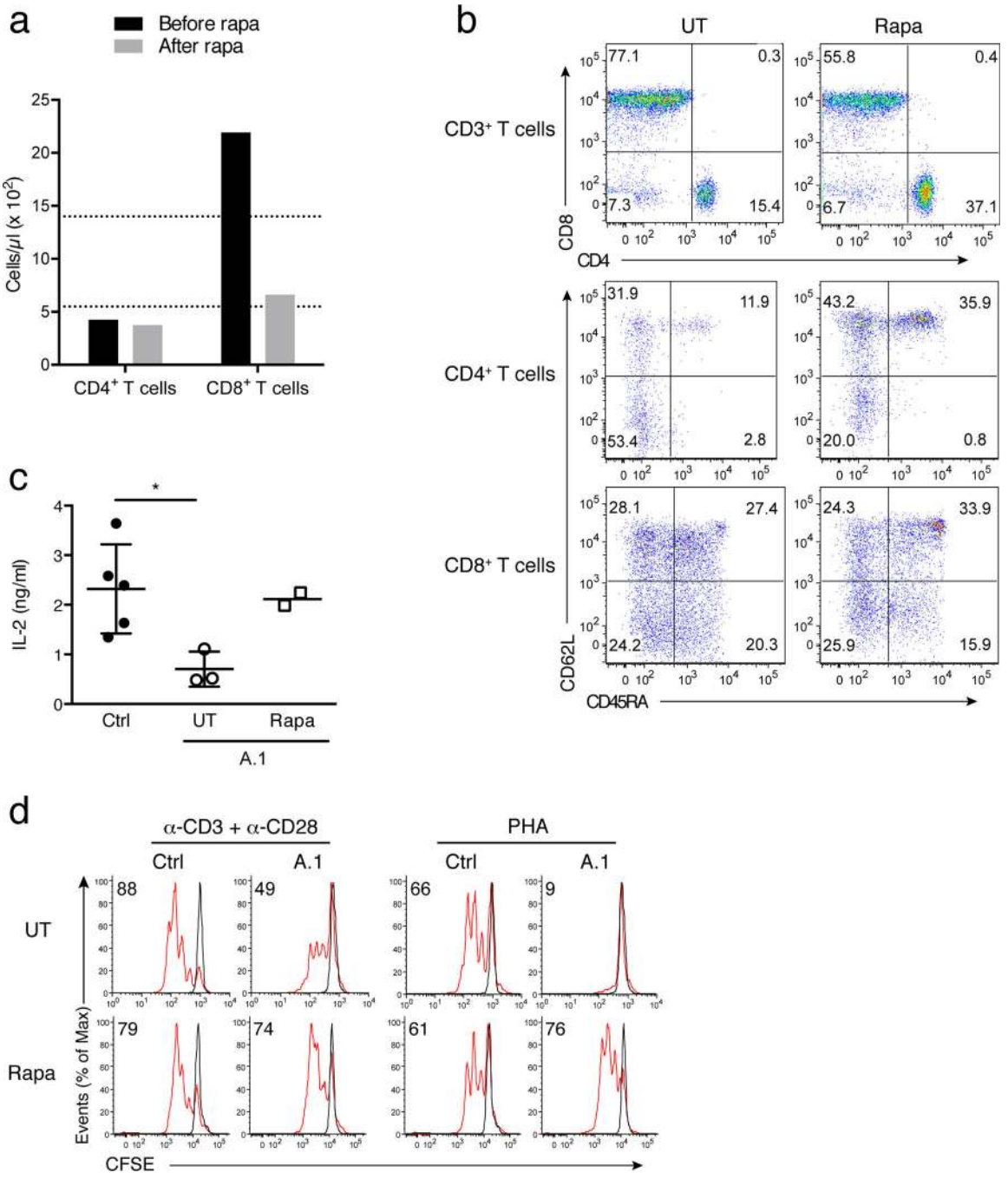

Figure 5. *In vivo* rapamycin treatment improves *in vitro* and *in vivo* disease phenotypes

(a) CD4$^+$ and CD8$^+$ T cell counts from patient A.1 before and after rapamycin treatment. Dotted lines represent the range of T cell counts for normal controls. **(b)** PBMCs from patient A.1 before (UT, untreated) and after *in vivo* rapamycin treatment (Rapa) displaying CD8$^+$ versus CD4$^+$ (CD3$^+$ gate, top) and CD62L versus CD45RA (CD4$^+$ gate, middle, or CD8$^+$ gate, bottom). Numbers in quadrants represent the percentage of total. **(c)** *In vitro* IL-2 production measured by Luminex after 24-hr activation (anti-CD3/CD28 Dynabeads) of PMBCs from an untreated normal control ($n = 5$) or patient A.1 before (UT, $n = 3$

independent measurements) rapamycin treatment (Rapa, left) and after ($n = 2$ independent measurements, right). Horizontal line indicates mean value, and $P = 0.04$ by the Mann-Whitney test. **(d)** Cell proliferation measured by CFSE dilution 72 hrs after activation (red) or not (black) of patient or control PBMCs with the indicated stimulus, shown before (UT, top) and after (bottom) *in vivo* treatment of patient A.1 with rapamycin (Rapa). The percentage of cells that have divided is shown.

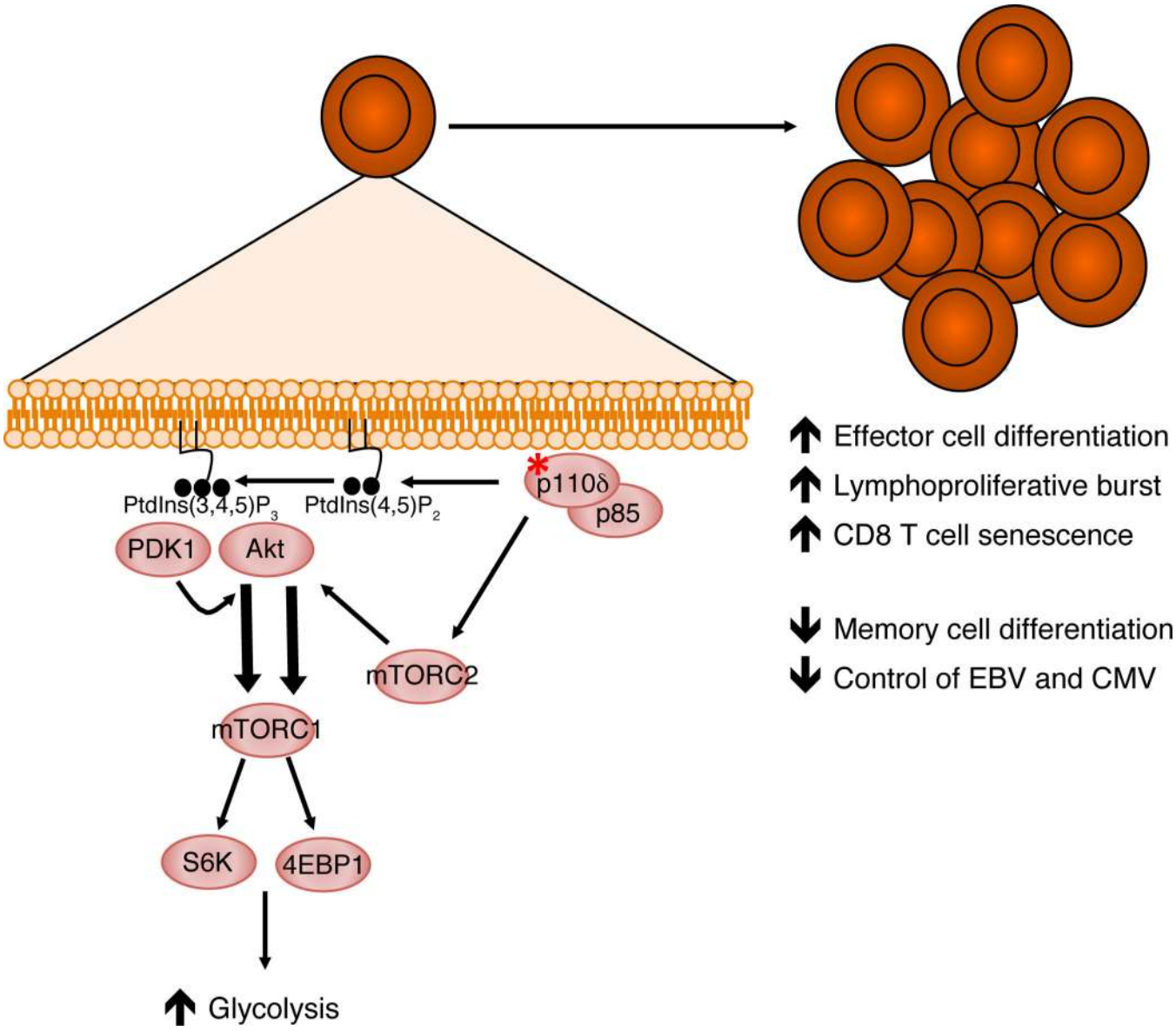

Figure 6. Proposed model of effects of activating mutations (red asterisk) in p110δ

Augmented PI(3)K signaling results in increased glycolysis, causing $CD8^+$ T cells to differentiate into effector cells that proliferate vigorously and then senesce. This results in impaired generation of long-lived memory $CD8^+$ T cells and, consequently, poor control of EBV and CMV infection.

Nat Immunol. Author manuscript; available in PMC 2014 October 27.

Table 1

Infections, lymphoma, lymphoproliferation, and immune phenotype in patient cohort

	Kinase Domain			Helical Domain					C2 Domain
	A.1	**B.III.1**	**C.1**	**D.I.1**	**D.II.1**	**D.II.2**	**E.1**	**F.II.1**	**G.1**
AGE, GENDER	12, M	14, F	15 (deceased), F	40, M	15, M	12, F	7, F	17, F	12, F
EBV VIREMIA	✔	✔	✔	✔	✔	✔	✔	✔	✔
CMV	✔	Naïve	N.D.	✔	✔	✔	✔	Naïve	Naïve
SINO-PULMONARY BACTERIAL INFECTIONS	✔	✔	✔	✔	✔	✔	✔	✔	✔
LYMPHOMA DIAGNOSIS	NO	*NO	EBV+ diffuse B cell lymphoma	NO	NO	NO	NO	EBV+ nodular sclerosis Hodgkin's	NO
LYMPH-ADENOPATHY	✔	✔	✔	NO	✔	NO	✔	✔	✔
MUCOSAL LYMPHOID AGGREGATES	✔	N.D.	N.D.	✔	✔	✔	✔	N.D.	✔
T & B LYMPHOCYTE SUBSETS	CD4 ↓ CD4 naïve ↓ CD8 CM, EM↑ CD5/CD20 ↑ Bmem switch ↓	CD4 ↓ CD4 naïve ↓ CD8 effector ↑ CD5/CD20 ↑ Bmem switch ↓	CD4 ↓ CD4 naïve ↓ CD8 effector ↑ CD5/CD20 ↑ N.D.	CD4 ↓ CD4 naïve ↓ CD8 EM ↑ CD5/CD20 ↑ Bmem switch **nl**	CD4 ↓ CD4 naïve ↓ CD8 CM, EM ↑ CD5/CD20 ↑ Bmem switch ↓	CD4 ↓ CD4 naïve ↓ CD8 CM, EM **nl** CD5/CD20 ↑ Bmem switch **nl**	CD4 ↓ CD4 naïve ↓ CD8 EM ↑ CD5/CD20 ↑ Bmem switch ↓	CD4 **nl** CD4 naïve **nl** CD8 CM, EM ↑ CD5/CD20 ↑ Bmem switch ↓	CD4 ↓ CD4 naïve ↓ CD8 EM ↑ CD5/CD20 ↑ Bmem switch ↓
TREGs**	Nl	nl	nl	N.D.	N.D.	N.D.	↑	nl	↓
CD3/8/57	44%	N.D.	42%	N.D.	35%	N.D.	N.D.	N.D.	41%
NK CELLS	NK **nl** NKT **nl**	NK **nl** NKT **nl**	NK **nl** NKT **nl**	NK ↓ NKT ↑	NK ↓ NKT ↓	NK **nl** NKT **nl**	NK ↑ NKT ↑	NK **nl** NKT **nl**	NK **nl** NKT **nl**
Ig	IgG↓, IgA↓ IgM↑	IgG **nl**, IgA **nl** IgM↑	rIgG↓, IgA↓ IgM↓	IgG↑, IgA **nl** IgM **nl**	IgG↓, IgA↓ IgM **nl**	IgG↑, IgA↓ IgM **nl**	**nl**	IgG **nl** IgA↓ IgM **nl**	IgG↓IgA↓ IgM↑

N.D. = not determined. nl = normal. M = male. F = female. Bmem = memory B cell.

*Family history of B cell lymphoma.

**Other T helper subsets including have been detected at normal frequencies.